Chemical Engineering Science 191 (2018) 100–114

Contents lists available at ScienceDirect

Chemical Engineering Science

journal homepage: www.elsevier.com/locate/ces

One-dimensional model of entrained-flow carbonator for CO_2 capture in cement kilns by Calcium looping process

Maurizio Spinelli, Isabel Martínez, Matteo C. Romano *

Politecnico di Milano, Department of Energy, via Lambruschini 4, 20156 Milan, Italy

HIGHLIGHTS

- Effect of design and operating parameters on CO_2 capture efficiency investigated.
- Calcined raw meal used as sorbent in the carbonator of the CaL process.
- High solid-to-gas ratio (~10 kg/Nm^3) needed to achieve high capture efficiency.
- Adiabatic carbonator suitable for achieving high capture efficiency.
- Carbonator solids recirculation allows limiting specific heat duty for regeneration.

GRAPHICAL ABSTRACT

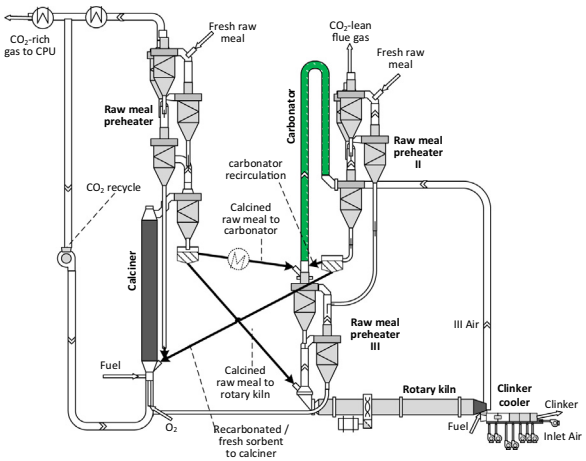

ARTICLE INFO

Article history:
Received 31 December 2017
Received in revised form 7 May 2018
Accepted 20 June 2018
Available online 21 June 2018

Keywords:
Ca-looping
CCS
Cement
Entrained flow reactor
Carbonator

ABSTRACT

In this work, a 1D model of an entrained-flow carbonator of a Calcium looping process for cement plants is presented and the results of a sensitivity analysis on the main governing process parameters is discussed. Several design and operating parameters have been investigated through a wide sensitivity analysis, namely: adiabatic vs. cooled reactor, high gas velocity gooseneck reactor vs. low velocity down-flow reactor, solid-to-gas ratio, sorbent capacity, reactor inlet temperature and solids recirculation. The effect of these design and process parameters on the CO_2 capture efficiency and on Calcium looping process heat consumption is assessed.

The results of the calculations showed that with a proper combination of solid-to-gas ratio in the carbonator and sorbent carbonation capacity (e.g. ~10 kg/Nm^3 and ~20% respectively), carbonator CO_2 capture efficiencies of about 80% (i.e. total cement kiln CO_2 capture efficiencies higher than 90%) can be obtained in a gooseneck-type carbonator with a length compatible with industrial applications in cement kilns (~120 to 140 m). Further experimental investigations on this reactor concept, especially about fluid-dynamic behavior and the chemical properties of raw meal as CO_2 sorbent, are needed to demonstrate the technical feasibility of the proposed process.

* Corresponding author.
E-mail address: matteo.romano@polimi.it (M.C. Romano).

https://doi.org/10.1016/j.ces.2018.06.051
0009-2509/

Nomenclature

A	reactor cross section [m^2]
C_{CO_2}	CO_2 concentration in gas phase [kmol/m^3]
$C_{CO_2,eq}$	CO_2 concentration in gas phase at chemical equilibrium with CaO-$CaCO_3$ [kmol/m^3]
C_D	drag coefficient [–]
c_p	specific heat capacity [J/kg/K]
D	reactor diameter [m]
D_p	Particle diameter [m]
E_a	activation energy of carbonation reaction kinetics: 21,300 kJ/kmol (Grasa et al., 2009)
F_{Ca}	sorbent molar flow from the calciner to the carbonator [kmol/s]
F_{CO2}	CO_2 molar flow in the gas fed to the carbonator [kmol/s]
F_{fg}	gas-wall friction force per unit of reactor length [N/m]
F_{fs}	solid-wall friction force per unit of reactor length [N/m]
f_g	fanning friction factor [–]
F_{gs}	gas-solid drag force per unit of reactor length [N/m]
Fe	Fedorov number [–]
g	gravitational acceleration: 9.81 m/s^2
G_s	specific solid flow at carbonator outlet, per unit of reactor cross section [kg/s/m^2]
h	sensible enthalpy [J/kg]
h_{gs}	heat transfer coefficient between gas and solids [W/m^2/K]
I_G	gravitational acceleration sign index: +1 for upward flow, −1 for downward flow
k_s	intrinsic kinetic constant of carbonation reaction [m^4/kmol/s]
$k_{s,0}$	pre-exponential factor of carbonation reaction kinetics: $0.559 \cdot 10^{-5}$ m^4/kmol/s (Grasa et al., 2009)
L	length of the pore system in the particle [m/m^3]
L_0	length of the pore system in the particle after the first calcination: $4.16 \cdot 10^{14}$ m/m^3 (Grasa et al., 2009)
M	molar mass [kg/kmol]
$\dot{M}$	mole flow rate [kmol/s]
$\dot{m}$	mass flow rate [kg/s]
N_s	number of solid particles per unit of reactor volume [m^{-3}]
Nu_{gs}	Nusselt number related to the gas-solid heat transfer coefficient [–]
p	pressure [Pa]
Pr	Prandtl number [–]
Q_{calc}	heat required in the calciner for calcination of the carbonated sorbent per unit of CO_2 captured [J/kg_{CO2}]
$\dot{Q}_{carb}$	thermal power generated by the carbonation reaction [W]
$\dot{Q}_w$	thermal power transferred to the reactor walls [W]
$\dot{q}_{CO2,carb}$	thermal power associated to the enthalpy flow of the reacting CO_2 per unit of reactor length [W/m]
$\dot{q}_{gs}$	thermal power transferred from the gas to the solids per unit of reactor length [W/m]
$\dot{q}_{gw}$	thermal power transferred from the gas to the reactor wall per unit of reactor length [W/m]
$\dot{q}_{r,carb}$	thermal power associated to the carbonation reaction per unit of reactor length [W/m]
$\dot{q}_{sw}$	thermal power transferred from the solids to the reactor wall per unit of reactor length [W/m]
R	gas constant: 8.314 kJ/kmol/K
Re	Reynolds number of the gas in the reactor [–]
Re_p	particle Reynolds number [–]
S	specific surface area available for carbonation reaction in the particle [m^2/m^3]
S_0	specific surface area available for carbonation reaction after the first calcination: $42 \cdot 10^6$ m^2/m^3 (Grasa et al., 2009)
T	temperature [K]
T_R	reaction temperature [K]
u	velocity [m/s]
$\dot{w}_{gs}$	work per unit length made by the gas on the solids [W/m]
x	axial coordinate [m]
X	sorbent conversion degree [–]
$X_{carb,out}$	sorbent conversion degree at carbonator outlet [–]
X_{max}	sorbent conversion degree after the fast kinetically controlled period [–]

Greek letters

$\Delta h^0_{r,carb}$	standard enthalpy of the carbonation reaction: 4.068 MJ/kg_{CO2}
ε_p	particle porosity [$m^3_{void}/m^3_{particle}$]
ε_s	volumetric solid density [$m^3_{solids}/m^3_{reactor}$]
ε_g	void fraction [$m^3_{gas}/m^3_{reactor}$]
μ_g	gas viscosity [Pa · s]
ξ	volume fraction of potentially active solids (CaO and $CaCO_3$) in the total solid population [$m^3_{CaO\&CaCO3}/m^3_{solids}$]
ρ	density [kg/m^3]
ψ	particle structural parameter for random pore kinetic model

Acronyms

ASU	air separation unit
CaL	calcium looping
CPU	CO_2 purification unit

Subscripts

0	CaO particle property after the first calcination
calc	calciner
capt	captured
carb	carbonator
ch	choking condition
g	gas
in	inlet
s	solids
s,a	potentially active solids (CaO and $CaCO_3$)
t	terminal
w	wall

1. Introduction

Cement production is responsible for about 8% of global anthropogenic CO_2 emissions (Olivier et al., 2016) and for more than 10% of total industrial CO_2 emissions in the EU (ZEP, 2013). In a modern cement kiln, roughly two-thirds of the CO_2 emissions derive from the calcination of the limestone that is used as raw material for clinker production. The residual fraction is associated with the fuel combustion necessary to sustain the endothermic $CaCO_3$ calcination and to bring the raw meal to the high temperature needed for clinker formation. For this reason, the use of alternative carbon-free or carbon–neutral fuels does not allow achieving a significant reduction of the CO_2 emissions and CO_2 capture and storage (CCS) is the only way to effectively reduce emissions form the cement industry.

Among the different CO_2 capture technologies, Calcium looping (CaL) (Abanades et al., 2015; Dean et al., 2011) appears particularly promising for application in cement plants because:

- CaO sorbent originates from the same raw material used for clinker production. Therefore, differently from other post-combustion capture systems, no additional chemical substances (e.g. solvents or additional sorbents) are needed with respect to the materials already used in the cement plant.
- The rotary kiln and the clinker cooler, which are two key units of the clinker production process, can be operated as in conventional plants and retrofitability of existing kilns may therefore be simpler. In contrast, oxyfuel combustion, which is the other main technology candidate for CO_2 capture in cement plants (Hoenig et al., 2012), requires switching the rotary kiln to oxyfuel combustion, using recirculated CO_2 as cooling medium in the clinker cooler and ensuring a proper sealing to avoid excessive air in-leakages.
- Although increased fuel consumptions are expected due to the heat required for regenerating the CaO sorbent, the corresponding amount of high temperature heat can be efficiently recovered from the process to feed a heat recovery steam cycle, which can partly or totally compensate the electric consumptions for O_2 production and CO_2 compression in the CaL process.

As discussed in detail in (De Lena et al., 2017; Spinelli et al., 2017), two fundamental options have been proposed in the literature for integrating the CaL into an existing cement kiln. The first and most straightforward one is the tail-end CaL process configuration, where the CaL reactors are placed downstream the clinker burning line as a relatively independent unit and the carbonator treats the flue gas exiting the cement kiln preheater or the raw mill. In this end-of-pipe configuration, pure limestone can be used as make-up of the CaL process and the CaO-rich purge extracted from the CaL calciner can be mixed with the other correctives (SiO_2, Al_2O_3 and Fe_2O_3-based materials), milled and fed to the clinker burning line as a partly pre-calcined raw meal. In this integration approach, the CaL system can be based on fluidized bed reactors, whose operating principle has been widely assessed through process modelling (Martínez et al., 2016; Shimizu et al., 1999) and proven up to 1.7 MW_{th}-scale (Abanades et al., 2015; Arias et al., 2013; Kremer et al., 2013) for application in coal-fired power plants. More recently, the tail-end CaL process integration in cement kilns with fluidized bed reactors has been assessed with process simulation studies (Atsonios et al., 2015; De Lena et al., 2017; Ozcan et al., 2013) and demonstrated experimentally at 30 kW_{th} and 200 kW_{th} scale (Arias et al., 2017a; Hornberger et al., 2017). Thanks to the experience gained on fluidized bed CaL systems, the tail-end process configuration is characterized by low uncertainties, being sufficiently mature for scaling-up in the cement industry. Moreover, it has been demonstrated suitable for retrofitting of existing cement kilns, with small impact on the operation of the cement kiln (De Lena et al., 2017).

The second option is the highly integrated CaL process configuration (Fig. 1), where the carbonator of the CaL process is integrated in the preheating tower of the clinker burning line. The carbonator treats the flue gas from the rotary kiln after proper cooling and the calciner of the CaL process coincides with the cement kiln precalciner, which is operated in oxyfuel combustion mode (Marchi et al., 2012a, 2012b; Rodríguez et al., 2012; Romano et al., 2014). In this configuration, two fundamental differences can be highlighted with respect to the tail-end CaL configuration explained before: (i) calcined raw meal (i.e. CaO with other SiO_2, Al_2O_3 and Fe_2O_3 raw constituents) is preferably used as a source of CaO sorbent for the carbonator rather than pure limestone; (ii) because of the small particle size of the raw meal (d_{50} = 10–20 μm), cement

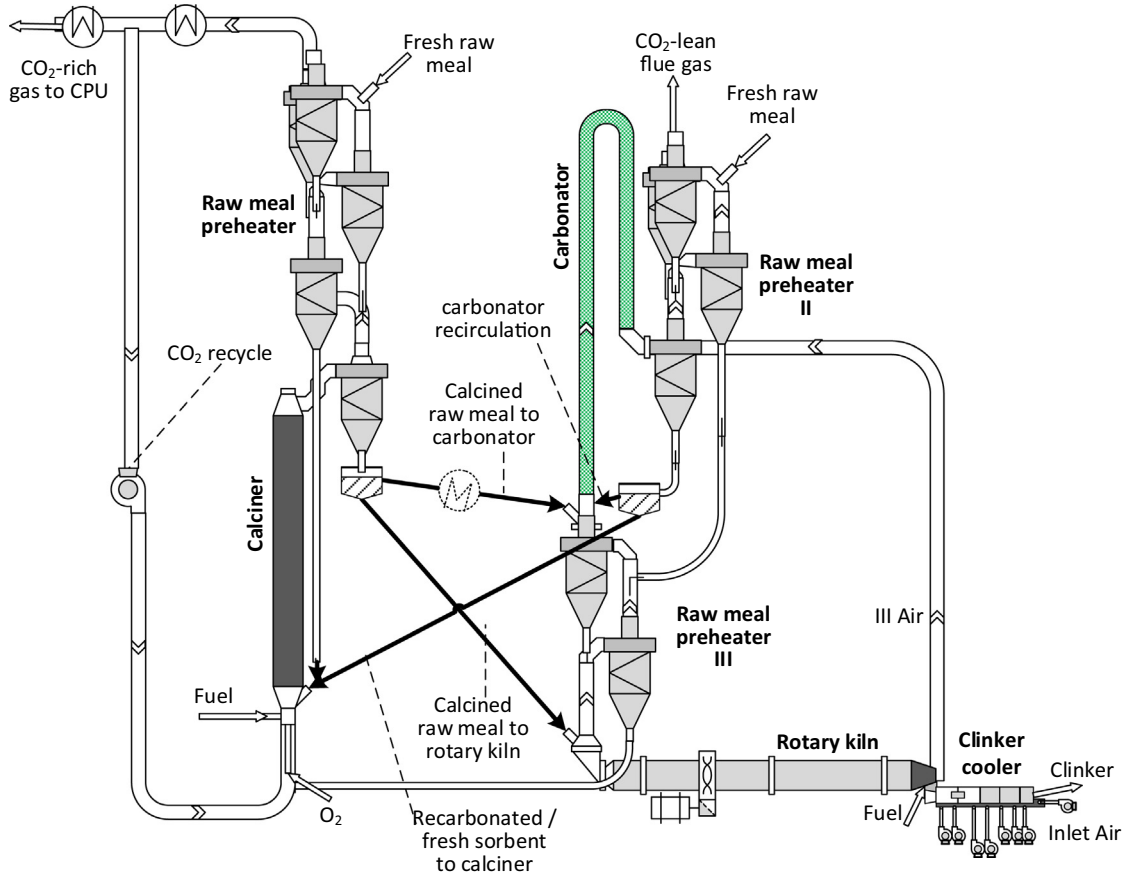

Fig. 1. Highly integrated CaL configuration with a gooseneck-type entrained flow carbonator.

raw meal falls in the region of cohesive particles (Geldart C particles (Geldart, 1973)) and entrained-flow reactors operating in the dilute pneumatic transport regime appear preferable over fluidized beds.

The main advantage of the highly integrated CaL process configuration is that it is expected to be more efficient than the CaL tail-end configuration thanks to the lower fuel consumption (Spinelli et al., 2017). Moreover, cement industry is experienced in operating entrained flow gas-solid systems (the pre-calciner and suspension preheaters of state-of-the-art cement kilns are entrained flow gas-solid reactors and contactors). On the other hand, there are higher uncertainties on the performance of this CaL system, which are mainly related to the performance of the calcined raw meal as CO_2 sorbent and to the fluid-dynamics of the entrained flow carbonator, which has to operate with much higher solid-to-gas ratio than conventional suspension preheaters.

Research on the performance of the calcined raw meal as CO_2 sorbent is ongoing. From lab tests it was found that both calcination conditions (temperature, CO_2 concentration and residence time) and the nature of the raw meal (especially the level of aggregation between Ca and Si compounds) influence the formation of belite (Ca_2SiO_4) in the calciner, which reduces the activity of the material towards CO_2 sorption (Alonso et al., 2017; Pathi et al., 2013). Further work is however needed in this field, where flash calcination conditions (i.e. residence times of few seconds) should be reproduced in the sorbent calcination step to evaluate the material sintering and the formation of calcium-silicate species under industrially relevant conditions.

The aim of this work, which is part of the CaL development activities performed within the H2020 Cemcap project (Cemcap, 2015), is to describe a reactor model developed for the entrained flow carbonator of an integrated CaL configuration and to evaluate the effect of the main process and reactor design parameters on the CO_2 capture efficiency of the carbonator through a sensitivity analysis. Two different reactors configurations are also assessed in this work, namely the high velocity gooseneck-type reactor, widely adopted in the cement industry for some calciner designs and formed by an upflow and a downflow section (Fig. 1), and a lower velocity downflow reactor (Fig. 2). Also, the performance obtained when having an externally cooled carbonator by waterwalls or an adiabatic carbonator are compared.

2. Method

A one-dimensional, steady-state model has been developed for the calculation of the entrained flow carbonator. The routine solves mass, energy and momentum balances along the axial direction for the gas and solid phases, providing cross-sectional averaged values of their chemical composition, temperature and velocity.

The main assumptions used to build the model are listed below:

- The gas phase is modelled with the ideal gas equation of state.
- Since the reactor operates with a dilute suspension (in the simulations performed in this work, the void fraction is always higher than 0.98), particle–particle interactions are neglected in the calculation of the momentum balance.
- The mass and momentum diffusion and the conductive heat flux along the axial direction are neglected.

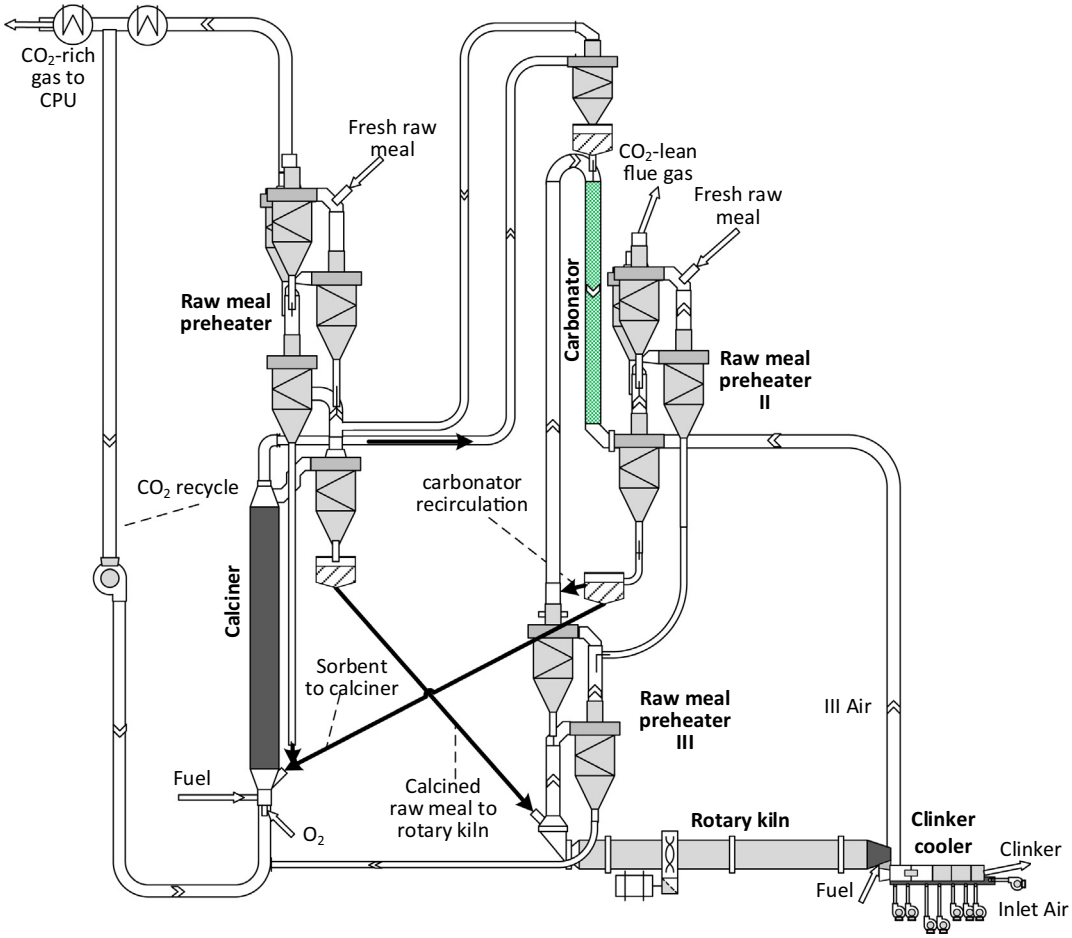

Fig. 2. Highly integrated CaL configuration with a downdraft entrained flow carbonator.

– Uniform temperature is considered for the solid throughout the particle.

It must be remarked that a simple fluid-dynamic modelling approach is selected for the model to allow fast calculations and wide sensitivity analysis. Moreover, because of the lack of proper experimental data on entrained flow reactors operating in conditions relevant for this study (especially combining pulverized particles, high solid/gas ratio and relatively large reactor diameters), it is believed that more complex modelling approach is not justified at this stage.

2.1. Mass balance

Mass balance of solid and gas phases is described by Equations (1) and (2), where the change of flow rate along the reactor length is related to the mass flow rate of CO_2 absorbed by the sorbent through the carbonation reaction $CaO + CO_2 \rightarrow CaCO_3$ ($\Delta H_{298\ K} = -178.8$ kJ/mol). In detail, Eq. (1) states that the variation of solids mass flow rate $d\dot{m}_s$ is equal to the number of moles of active sorbent in an infinitesimal control volume $A \cdot dx \cdot \frac{\varepsilon_s \cdot \xi \cdot \rho_{s,a}}{M_{s,a}}$, multiplied by the sorbent molar conversion rate $\frac{dX}{dt}$ and the CO_2 molar mass M_{CO2}.

$$\frac{d\dot{m}_s}{dx} = A \cdot \frac{\varepsilon_s \cdot \xi \cdot \rho_{s,a}}{M_{s,a}} \cdot \frac{dX}{dt} \cdot M_{CO2} = \frac{\xi \cdot \dot{m}_s \cdot \rho_{s,a}}{u_s \cdot \rho_s \cdot M_{s,a}} \cdot \frac{dX}{dt} \cdot M_{CO2} = \frac{\dot{M}_{s,a}}{u_s} \cdot \frac{dX}{dt} \cdot M_{CO2} \quad (1)$$

$$\frac{d\dot{m}_g}{dx} = -\frac{d\dot{m}_s}{dx} \quad (2)$$

For the sorbent conversion rate, the random pore model Equation (3) proposed by Grasa et al. (2009) is used, which describes the sorbent reaction rate in the fast kinetically controlled period. The use of this equation, neglecting the diffusion-controlled particle conversion, is justified given the small particle size of the material used as sorbent in this case (i.e. average particle diameters of 10–20 μm) and the reduced residence time of the particles in the entrained flow reactor. In Eq. (3), k_s represents the intrinsic kinetic constant of the carbonation reaction, which is calculated as function of temperature with the Arrhenius type Eq. (4). Reaction temperature T_R is assumed equal to the local adiabatic mixing temperature between the gas and the solid stream. In the random pore model, ψ represents a particle structural parameter (Eq. (5)), S is the surface area available for reaction in the particle, L is the length of the pore system in the particle and ε_p is the particle porosity. Particle surface area and length of the pore system are calculated with Equations (6) and (7) as function of the initial surface S_0 and pore length L_0 and of the conversion degree of the sorbent after the kinetic controlled period X_{max}. In conventional CaL systems using high purity limestone as sorbent, X_{max} is typically expressed as function of the number of calcination-carbonation cycles undergone by a sorbent particle, with a limited dependency on the origin of the limestone (Grasa and Abanades, 2006). However, when raw meal is used as CO_2 sorbent in a CaL system, lab tests showed that the maximum sorption capacity is highly dependent on the calcination conditions and on the nature of the CaO-based material. These variables determine the advancement of the reaction in the calciner between Ca and SiO_2 in the raw meal and therefore the amount of free CaO available as sorbent in the carbonator (Alonso et al., 2017; Arias et al., 2017b). Due to the lack of laboratory tests reproducing realistic calcination conditions of cement kiln pre-calciners for CaL, it is not currently possible to define a reliable correlation for predicting the parameter X_{max}, which has been therefore given as a simulation input in this work and is subject of sensitivity analysis. It has to be highlighted that the assumed values of X_{max} are always lower than those predicted with the expression of the capacity decay with the number of calcination/carbonation cycles proposed in (Grasa and Abanades, 2006) for a wide number of high purity limestones. It must also be highlighted that it has been observed that reaction rates found in several experimental works on high purity limestones are representative of the carbonation kinetics of calcined raw meals as long as the fraction of active CaO in the solids able to react in the fast carbonation regime X_{max} is known (Arias et al., 2017b).

The driving force of the carbonation reaction is the difference between the actual CO_2 concentration C_{CO_2} in the gas phase and the CO_2 concentration $C_{CO_2,eq}$ at thermodynamic equilibrium with CaO, calculated as function of temperature with the equation proposed in (Barker, 1973). The process is assumed to be under full chemical control, meaning that carbonation kinetics represents the rate determining step and the convective and diffusive mass transfer resistance from the bulk to the particle surface are neglected. The validity of this assumption has been verified by checking that the local CO_2 flux due to CO_2 diffusion in gas phase is at least 10 times larger than the CO_2 flux due to the chemical reaction.

For the description of the other symbols in Equations (3)(6) and the values assumed in the simulations, the reader is addressed to the nomenclature list.

$$\frac{dX}{dt} = \frac{k_s \cdot S}{1-\varepsilon_p} \cdot (1-X) \cdot \sqrt{1 - \psi \cdot ln(1-X)} \cdot (C_{CO_2} - C_{CO_2,eq}) \quad (3)$$

$$k_s = k_{s,0} \cdot \exp\left(\frac{-E_a}{R \cdot T_R}\right) \quad (4)$$

$$\psi = \frac{4\pi \cdot L \cdot (1-\varepsilon_p)}{S^2} \quad (5)$$

$$S = S_0 \cdot X_{max} \quad (6)$$

$$L = L_0 \cdot X_{max} \quad (7)$$

In addition to the mass balance Eqs. (1) and (2), continuity Eqs. (8) and (9) relate the gas and solids velocities with the cross-section surface area occupied by the gas (A_g) and by the solids (A_s), while Eq. (10) relates these areas with the total reactor cross section area and the solid volumetric density ε_s.

$$\dot{m}_g = u_g \cdot \rho_g \cdot A_g \quad (8)$$

$$\dot{m}_s = u_s \cdot \rho_s \cdot A_s \quad (9)$$

$$A = A_g + A_s = A \cdot (1-\varepsilon_s) + A \cdot \varepsilon_s \quad (10)$$

2.2. Momentum balance

Momentum balance is written for the gas and the solid phases as shown in Eqs. (11) and (12), following the approach of Rajan et al. (Rajan et al., 2006). In these equations I_G is an index representing the sign of the gravitational acceleration with respect to the flow direction and it is equal to +1 in case of upward flow and −1 in case of downward flow, F_{fg} and F_{fs} are the gas-wall and the solid-wall friction forces and F_{gs} is the gas-solid drag force per unit of reactor length.

$$\frac{d(\dot{m}_g \cdot u_g)}{dx} + A \cdot \frac{dp}{dx} = -I_G \cdot A_g \cdot \rho_g \cdot g - F_{fg} - F_{gs} \quad (11)$$

$$\frac{d(\dot{m}_s \cdot u_s)}{dx} = -I_G \cdot A_s \cdot \rho_s \cdot g - F_{fs} + F_{gs} \quad (12)$$

Gas-wall friction force F_{fg} is calculated with Eq. (13), with the Fanning friction factor f_g for smooth circular tubes that is calculated through Eq. (14) (Drew et al., 1932). In case of the gooseneck carbonator, an additional localized pressure drop at the 180° bend at the top of the reactor has been calculated with the Chambers and Marcus correlation (Eq. (15)) (Chambers and Marcus, 1986). Solid-wall friction forces are computed for the vertical flow reactor sections with the Konno-Saito Eq. (16) (Konno and Saito, 1969). For the calculation of the gas-solid drag force F_{gs}, Eq. (17) has been used, where the drag coefficient C_D is obtained as a function of the particle Reynolds number (Eq. (18)) by Eq. (19) (Rhodes, 2008).

$$F_{fg} = 2 \cdot f_g \cdot \rho_g \cdot u_g^2 \cdot \frac{A_g}{D} \tag{13}$$

$$f_g = 0.0014 + \frac{0.125}{Re^{0.32}} \tag{14}$$

$$\Delta p_{bend} = \frac{3 \cdot \left(1 + \frac{\dot{m}_s}{\dot{m}_g}\right) \cdot \rho_g \cdot u_g^2}{2} \tag{15}$$

$$F_{fs} = 0.057 \cdot \dot{m}_s \cdot \sqrt{\frac{g}{D}} \tag{16}$$

$$F_{gs} = \frac{3 \cdot C_D \cdot A_s \cdot \rho_g \cdot A^{0.65} \cdot (u_g - u_s) \cdot |u_g - u_s|}{4 \cdot D_p \cdot A_g^{0.65}} \tag{17}$$

$$Re_p = \frac{\rho_g \cdot |u_g - u_s| \cdot D_p}{\mu_g} \tag{18}$$

$$\begin{cases} C_D = \frac{24}{Re_p}, & Re_p < 0.3; \\ C_D = \frac{24}{Re_p} \cdot (1 + 0.15 \cdot Re_p)^{0.687}, & 0.3 < Re_p < 500 \\ C_D = 0.44, & Re_p > 500 \end{cases} \tag{19}$$

In order to check that pneumatic transport regime is maintained throughout the reactor length without flow instability, in each section of the reactor with upward flow, choking gas velocity is calculated and compared with the actual one. In fact, if choking conditions were reached, solid particles would start a backflow motion and the model equations would not properly represent the flow field. Choking gas velocity $u_{g,ch}$ and void fraction ε_{ch} at choking conditions are calculated with the system of Eqs. (20) and (21) (Rhodes, 2008) as a function of the solid mass flow rate, the particle density, the reactor geometry and the particle terminal velocity (u_t).

$$\frac{u_{g,ch}}{\varepsilon_{g,ch}} - u_t = \frac{\dot{m}_s / A}{\rho_s \cdot (1 - \varepsilon_{g,ch})} \tag{20}$$

$$\rho_g^{0.77} = \frac{2250 \cdot D \cdot (\varepsilon_{g,ch}^{-4.7} - 1)}{\left(\frac{u_{g,ch}}{\varepsilon_{g,ch}} - u_t\right)^2} \tag{21}$$

2.3. Energy balance

Energy balance is written for the gas and the solid phases as shown in Eqs. (22) and (23). Changes of total energy of the gas and solid phases per unit of reactor length are related to the work per unit length made by the gas on the solids ($\dot{w}_{gs}$), to the thermal power transferred from the gas to the solids ($\dot{q}_{gs}$), from the gas to the reactor wall ($\dot{q}_{gw}$) and from the solids to the reactor wall ($\dot{q}_{sw}$) per unit of reactor length, to the thermal power generated by the carbonation reaction ($\dot{q}_{r,carb}$) and to the enthalpy flow associated to the reacting CO_2 ($\dot{q}_{CO2,carb}$).

$$\frac{d(\dot{m}_g \cdot h_g + 0.5 \cdot \dot{m}_g \cdot u_g^2 + I_G \cdot \dot{m}_g \cdot g \cdot x)}{dx} = -\dot{w}_{gs} - \dot{q}_{gw} - \dot{q}_{gs} - \dot{q}_{CO2,carb} \tag{22}$$

$$\frac{d(\dot{m}_s \cdot h_s + 0.5 \cdot \dot{m}_s \cdot u_s^2 + I_G \cdot \dot{m}_s \cdot g \cdot x)}{dx} = \dot{w}_{gs} - \dot{q}_{sw} + \dot{q}_{gs} + \dot{q}_{r,carb} + \dot{q}_{CO2,carb} \tag{23}$$

In Eqs. (22) and (23), h refers to the sensible enthalpy of gas and solids (Eq. (24)), where the specific heat capacity is calculated with 4th degree NASA polynomials function of temperature (Gardiner, 1984), regressed against data in (NASA ThermoBuild, 2017; Stull and Prophet, 1971). The reaction heat term is calculated from the standard enthalpy of the carbonation reaction ($\Delta h^0_{r,carb}$) and from the solids mass flow rate change, as shown in Eq. (25). As indicated in the energy balance equation for the solid phase (Eq. (23)), heat of carbonation reaction is assumed to be released entirely on the solid phase. The enthalpy flow associated to the reacting CO_2, which is removed from the gas phase and transferred to the solid phase, is calculated with Equation (26).

$$h = \int_{298K}^{T} c_p \cdot dT \tag{24}$$

$$\dot{q}_{r,carb} = \frac{d\dot{m}_s}{dx} \cdot \Delta h^0_{r,carb} \tag{25}$$

$$\dot{q}_{CO2,carb} = \frac{d\dot{m}_s}{dx} \cdot h_{CO2} \tag{26}$$

The work made by the gas on the solids is computed with Equation (27).

$$\dot{w}_{gs} = u_s \cdot F_{gs} \tag{27}$$

Gas to solids heat transfer is calculated with Eq. (28), where N_s is the number of solid particles per unit of reactor volume, calculated with Eq. (29). Only convective heat transfer is considered in the model to calculate the gas-solid heat transfer coefficient h_{gs}, which is estimated with empirical Equation (30) (Rajan et al., 2008), where Fe is the Fedorov number (Eq. (31)).

$$\dot{q}_{gs} = A \cdot N_s \cdot \pi \cdot D_p^2 \cdot h_{gs} \cdot (T_g - T_s) \tag{28}$$

$$N_s = \frac{6 \cdot A_s}{A \cdot \pi \cdot D_p^3} \tag{29}$$

$$Nu_{gs} = 8.2951 \cdot 10^{-7} \cdot Re_p^{5.3365} \cdot \left(\frac{\dot{m}_s}{\dot{m}_g}\right)^{-1.3863} \cdot Fe^{-5.053} \tag{30}$$

$$Fe = D_p \cdot \left[\frac{4 \cdot g \cdot \rho_g^2}{3 \cdot \mu_g^2} \cdot \left(\frac{\rho_s}{\rho_g} - 1\right)\right]^{1/3} \tag{31}$$

Regarding the thermal power transferred from the gas and the solid phases to the reactor wall, the particles-to-wall heat transfer ($\dot{q}_{sw}$) is assumed zero due to the very low solid fraction in the reactor, while the thermal power transferred from the gas phase to the reactor wall ($\dot{q}_{gw}$) is calculated with Eq. (32), which includes the enhancement provided by the presence of the solid particles. Gas-to-wall heat transfer coefficient h_{gw} is computed from Nu_{gw} in Eq. (33), where the first term between brackets from the Dittus-Boelter correlation is increased by the second term that includes the ratio of the heat capacities of solids and gas streams (Pfeffer et al., 1966).

$$\dot{q}_{gw} = A \cdot h_{gw} \cdot (T_g - T_w) \tag{32}$$

$$Nu_{gw} = (0.023 \cdot Re^{0.8} \cdot Pr^{0.3}) \cdot (1 + 4 \cdot Re^{-0.32} \cdot \frac{\dot{m}_s}{\dot{m}_g} \cdot \frac{c_{p,s}}{c_{p,g}}) \quad (33)$$

Viscosity and thermal conductivity of the gas needed for the calculation of the heat transfer coefficients, the Reynolds and Prandtl numbers are taken from (Incropera et al., 2007).

In the proposed modelling approach, thermal power transferred from the gas-solid mixture to the reactor wall does not include the contribution of heat transfer by radiation. As quantitatively discussed further on, the contribution of heat transfer by radiation from the particles to the wall would be non-negligible if particles are considered at the bulk temperature. However, as discussed by (Danziger, 1963) for fluid catalytic cracking risers operating with solid densities and temperatures relevant for this study, it is reasonable to expect that particles involved in the heat transfer by radiation are those flowing in the gas film close to the wall at temperature significantly lower than the bulk. Therefore, radiation from the bulk stream is expected to be shielded by the particles in the film, which radiate the tube wall at lower temperature, and heat transfer by radiation is considered negligible compared to heat transfer by convection (Danziger, 1963). In this work, in order to keep a simple modelling approach and avoid model complexity not supported by proper experimental data, radiation is not included in the model. However, the effects of increased heat transfer coefficients, possibly due to radiation, are discussed through a sensitivity analysis in the results section.

2.4. Solution of model equations

A forward finite difference method has been implemented in Matlab (The Mathworks Inc.) to solve the equations along the reactor length.

Mass flow rate, temperature, pressure and composition of the gas and solid phases at the entrance section are given as input, together with the reactor cross section. A constant wall temperature T_w in the case of a water-cooled reactor or an adiabatic operation mode can be given as boundary conditions for calculating the gas-to-wall heat flux. In case of a cooled reactor, the assumption of a constant wall temperature, close to the cooling fluid temperature, is justified by the much higher heat transfer coefficient expected for the coolant (evaporating water) compared to the reacting mixture inside the reactor.

The possibility of operating the entrained-flow carbonator with solid recirculation (i.e. recycling a portion of the solids collected by the cyclone at carbonator outlet back to the inlet of the reactor) is implemented. In this case, an iterative calculation is implemented, where solid composition and flow rate at the inlet section are updated until convergence is achieved (i.e. 0.1% allowable difference of solid and gas flow rates at carbonator outlet between two consecutive iterations).

The main output of the model is the CO_2 capture efficiency profile along the reactor. Provided that the carbonation reaction is the only reaction considered in the model, CO_2 capture efficiency is univocally related to the gas mass flow rate and is calculated with Eq. (34).

$$E_{CO2} = 1 - \frac{\dot{m}_{CO2}}{\dot{m}_{CO2,in}} = \frac{\dot{m}_{g,in} - \dot{m}_g}{\dot{m}_{CO2,in}} \quad (34)$$

2.5. Sensitivity analysis

A sensitivity analysis has been performed on the entrained-flow CaL system. Baseline assumptions and the range of variation of some significant model parameters in the sensitivity analysis are reported in Table 1. Flow rate and CO_2 concentration of the gas from the rotary kiln to be treated in the carbonator are defined based on the mass balances of the reference cement kiln defined in Cemcap (Campanari et al., 2016).

Maximum CaO conversion (X_{max}) of 0.2 at the end of the kinetic controlled conversion period has been assumed as baseline. As previously discussed, the actual maximum CaO conversion in an industrial installation is expected to be highly dependent on the nature of the raw meal and on the calcinations conditions. For this reason, it is difficult to predict the sorbent capacity with the current knowledge and experimental data and a sensitivity analysis has been performed on this parameter, which is modified in the 0.1–0.3 range.

The assumed gas velocity at the inlet of the carbonator is 15 m/s and 4 m/s for the gooseneck and the downflow reactors, respectively. When the reactor inlet temperature of 600 °C is considered, these velocities correspond to a carbonator internal diameter of 1.8 m for the gooseneck reactor and of 3.6 m for the downflow reactor.

Gas and solid temperature at carbonator inlet is equal to 600 °C in the baseline conditions. To show the influence of this parameter on the carbonator performance, cases with a higher inlet temperature of 650 °C have been also calculated. When a cooled carbonator is considered, the reactor wall temperature is fixed at 300 °C that is considered a reasonable temperature for a reactor cooled by the evaporation of high pressure water.

Table 1
Assumptions for the simulation of the entrained flow CaL carbonator.

	Reference value	Range in sensitivity analysis
Gas flow rate, kg/s	17.06	
Nm^3/s	12.44	
CO_2 concentration in the gas, vol%	19.8	
Composition of calcined solids, wt%	65.5CaO, 0.2$CaCO_3$, 21.6SiO2, 5.0Al_2O_3, 2.7Fe_2O_3, 2.4MgO, 2.6$CaSO_4$	
Solids density, kg/m^3	CaO: 1660 $CaCO_3$: 2710 Other solids: 1830	
Maximum CaO conversion (X_{max})	0.20	0.10–0.30
Particle size, μm	30	
Gas inlet velocity, m/s – gooseneck reactor	15	
– downflow reactor	4	
Solids from calciner to gas ratio, kg/Nm^3	5	5–15
Carbonator solids recirculation,%	0	0–66.7
Initial solid velocity, m/s	1	
Reactants inlet temperature, °C	600	600–650
Reactor wall temperature (cooled carbonator only), °C	300	
Calciner outlet temperature, °C	920	

Finally, to calculate the heat needed in the calciner to sustain the CaL process, a calciner outlet temperature of 920 °C has been assumed. Energy consumption in the calciner of the CaL has been calculated considering the sensible heat needed for heating the solids from carbonator outlet temperature to the calciner outlet temperature and the calcination heat of the recarbonated raw meal from the carbonator. Heat needed for first heating and first calcination of the incoming raw meal from the preheater is not included in this calculation, being independent of the CaL process.

3. Results and discussion

In Fig. 3, the CO_2 capture efficiency along the gooseneck carbonator reactor is represented, considering both adiabatic and cooled reactors and different solid/gas ratio. A solid to gas ratio of around 10 kg/Nm^3 (vs. about 1–1.5 kg/Nm^3 of conventional preheaters) is needed in the carbonator to achieve a CO_2 capture efficiency of 80% (i.e. about 90% capture efficiency for the whole cement kiln) with a reactor length of 120–140 m. Moreover, operating with a cooled reactor allows achieving higher capture efficiencies, especially when 4 parallel cooled reactors with reduced cross-section are used to increase the reactor surface/volume ratio. Quantitatively, reactor cooling allows to increase the capture efficiency by about 6–8% points in case of 4 parallel reactors and by about 5–6% points in case of single cooled reactor, compared to the adiabatic reactor case.

The CO_2 capture enhancement achievable with a cooled reactor depends on the heat transfer coefficient, which is calculated to range from 19 to 21 W/m^{2}K with solid loading of 5 kg/Nm^3, to 22–24 W/m^{2}K with solid loading of 10 kg/Nm^3 and 26–28 W/m^{2}K with solid loading of 15 kg/Nm^3. As discussed in Section 2.3, the calculated heat transfer coefficient is somewhat underestimated by the model because heat transfer by radiation is neglected. If radiation from particles at 650 °C (indicative average bulk temperature along the reactor) to the wall at 300 °C both with emissivity of 0.85 is considered, equivalent heat transfer coefficient of about 75 W/m^{2}K can be calculated (i.e. roughly 3 times the estimated convective heat transfer coefficient). However, as discussed in Section 2.3, the actual heat transfer by radiation is expected to be much lower than this theoretical maximum, because of the shield effect of the colder particles flowing in the gas film next to the reactor wall. Because of the uncertainty related to this phenomenon, a sensitivity analysis has been performed on the value of the heat transfer coefficient for the single cooled reactor case with solid loading of 10 kg/Nm^3. For this case, if heat transfer coefficient is doubled (i.e. adding about 1/3 of the theoretical maximum heat flux by radiation and achieving overall heat transfer coefficient of 52–55 W/m^{2}K) CO_2 capture efficiency would rise from 83.8% to 87.2%, roughly reproducing the CO_2 capture efficiency vs. length curve obtained for the case with 4 parallel cooled reactors. If heat transfer coefficient is increased by a factor 4 (i.e. roughly adding the theoretical maximum heat flux by radiation and achieving overall heat transfer coefficient of 105–110 W/m^{2}K) CO_2 capture efficiency would achieve 88.4%.

In all the cases, even accounting for the uncertainty related to the heat transfer, it is believed that the improvement of the capture efficiency achievable with cooled carbonator does not justify the increased cost associated to a waterwall cooled reactor. Therefore adiabatic reactors are expected to be preferable from the techno-economic point of view.

In Fig. 4 temperature profiles of the cases shown in Fig. 3 are plotted as function of CO_2 capture efficiency (a) and reactor length (b). Monotonic temperature increase along the reactor length is observed for the adiabatic reactors. A virtually linear trend results in the temperature vs. CO_2 capture efficiency chart, since temperature increase is proportional to the carbonation reaction heat (non-visible non-linearity is only due to the dependency of the reaction heat and of the specific heat capacity on the temperature). A higher slope is obtained for the case with low solid/gas ratio because of the lower thermal inertia resulting from the lower solids flow rate. In case of cooled reactors, temperature curves show a non-monotonic trend, with a maximum obtained when the heat generated by the carbonation reaction is balanced by the heat exchanged with the reactor walls. This maximum temperature is achieved at lower CO_2 capture efficiencies in case of 4 parallel reactor because of the higher heat flux to the reactor walls. In the case with 4 parallel reactors, the lowest solid to gas ratio also shows the lowest temperature, differently from the adiabatic and the single cooled reactor cases. This is also due to the higher heat flux to the reactor walls, which balances the low heat generated by the carbonation reaction when there is a low amount of sorbent in the reactor, slowing down the carbonation reaction rate.

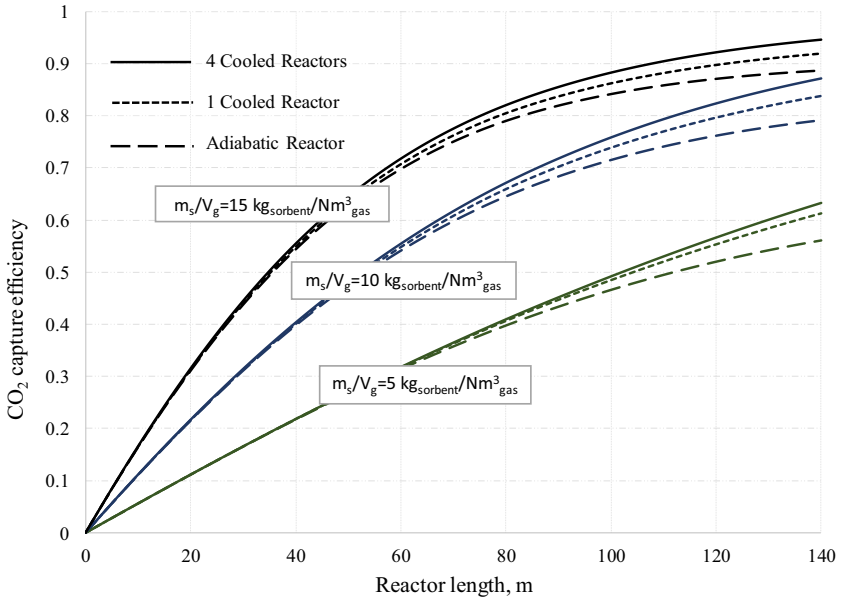

Fig. 3. CO_2 capture efficiency vs. reactor length, for adiabatic and cooled reactor and different solid/gas ratio (X_{max} = 20%, inlet temperature = 600 °C, no solids recycle).

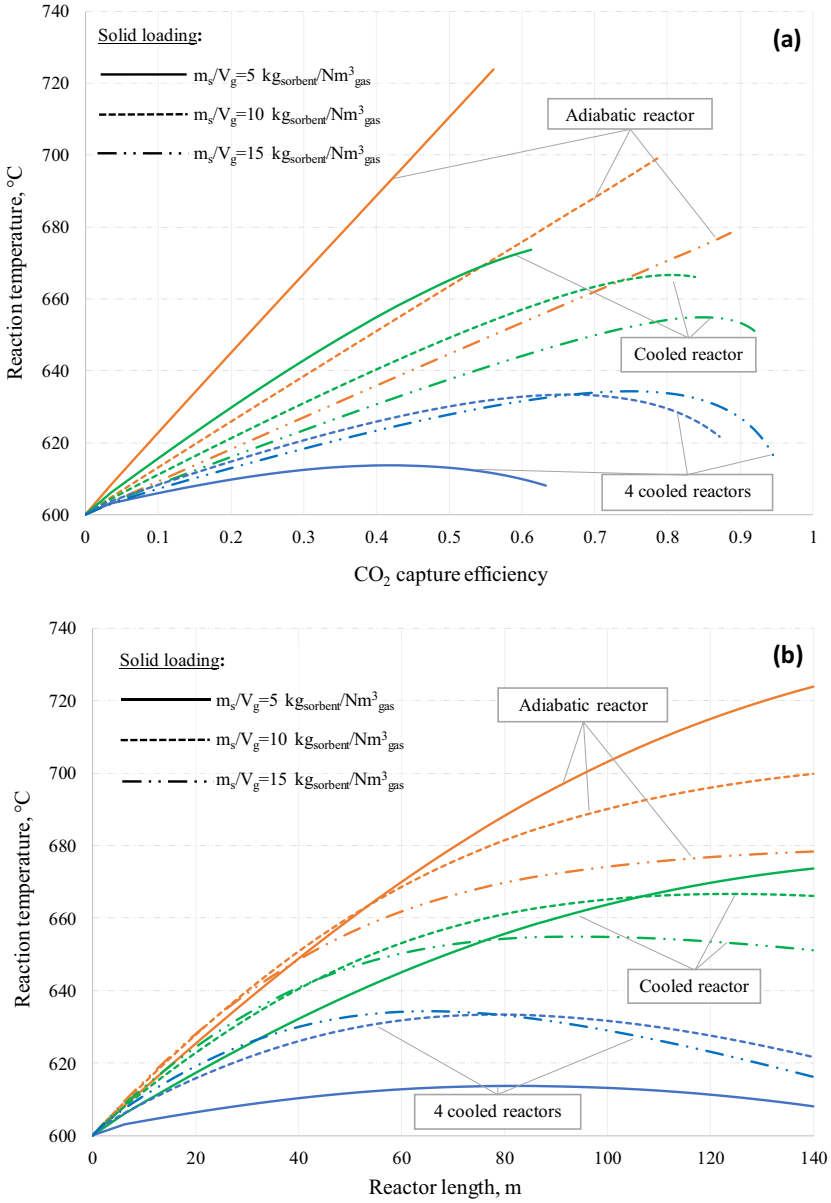

Fig. 4. Reaction temperature vs. CO_2 capture efficiency (a) and vs. reactor length (b), for adiabatic and cooled reactor and different solid/gas ratio (X_{max} = 20%, inlet temperature = 600 °C).

Interpretation of temperature profiles in the temperature-reactor length chart of Fig. 4b is less straightforward. In general, it can be observed that with the assumed sorbent conversion X_{max} of 0.2, a temperature increase of 80–100 °C can be expected in an adiabatic reactor with high capture efficiency. With 4 cooled reactors, temperature is relatively stable, showing a maximum temperature increase of about 30 °C along the reactor.

In Fig. 5, CaO conversion is reported as function of the reactor length for the same cases previously discussed. It can be observed that CaO conversion at reactor outlet is always far from the maximum conversion of 0.2. This indicates that in such conditions, CO_2 capture efficiency is not limited by sorbent capacity. Therefore, a higher sorbent utilization can be obtained by recirculating a fraction of the solids from the carbonator outlet back to the reactor inlet, increasing in this way their residence time and so their conversion.

Extended overall results of the CaL simulations are summarized in Table 2. Cases 1–9 correspond to cases without carbonator solids recirculation presented in the previous figures. Additional indicators are reported in this table, such as the specific solid flow at carbonator outlet (G_s), the carbonation reaction heat ($\dot{Q}_{carb}$) and the heat transferred to reactor walls ($\dot{Q}_w$). In the last line, the specific heat required in the calciner for sorbent regeneration per kg of captured CO_2 (Q_{calc}) is reported, which accounts for the heat needed for heating the carbonated solids up to the calciner temperature and for their calcination. It can be noted that higher specific heat consumptions are obtained compared to conventional fluidized bed CaL process for power plants or for cement plants with tail-end configuration (De Lena et al., 2017; Martínez et al., 2016), because raw meal is used in this process instead of high purity limestone, which requires additional heat for heating of the raw meal compounds other than CaO and $CaCO_3$, which do not participate in the CO_2 capture reaction.

From the results of cases 1–9 in Table 2, it is clear that regardless of the type of reactor, the higher the solids to gas ratio, the higher the specific heat demand in the calciner, since the

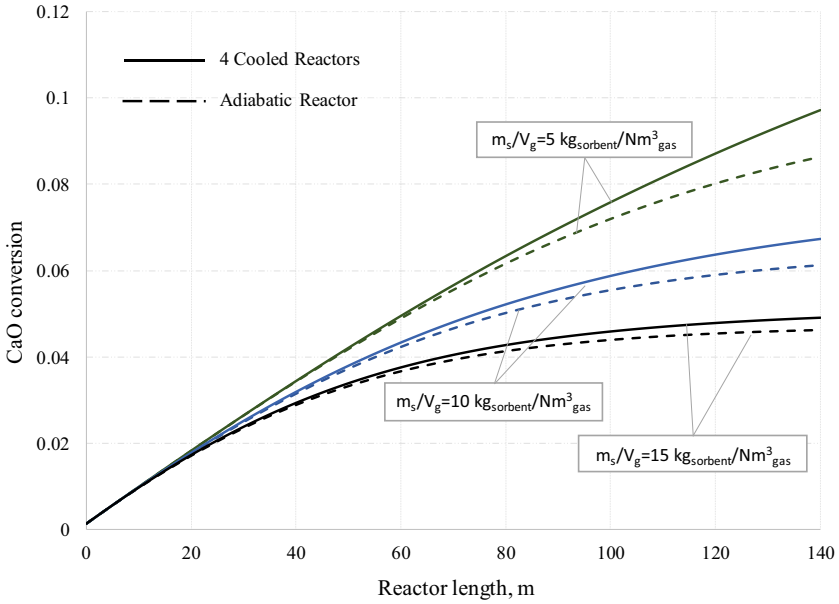

Fig. 5. CaO conversion vs. reactor length, for adiabatic and cooled reactor and different solid/gas ratio (X_{max} = 20%, inlet temperature = 600 °C).

conversion reached by the sorbent in the carbonator is reduced and there is a larger amount of inert solids circulating between the CaL reactors per kg of CO_2 captured. To keep a proper solid loading in the carbonator without increasing the solid flow from the calciner to the carbonator, carbonator solids recirculation can be adopted.

Fig. 6 shows the results obtained when X_{max} is equal to 0.20, solids circulation from calciner to carbonator is maintained at 5 kg/Nm^3 (or F_{Ca}/F_{CO2} of 6.6) and solid loading at carbonator inlet is increased up to about 10 and 15 kg/Nm^3 by recycling 1/2 and 2/3 of the solids at carbonator outlet. Temperature at carbonator inlet is kept at 600 °C, assuming that the recirculated solids are cooled from the carbonator outlet temperature to such inlet temperature. Overall results of the cases with adiabatic reactor are reported in Table 2 as cases 10–11. CO_2 capture efficiencies of 75.9 and 82.5% are obtained with solids recycle rate of 50 and 67% respectively, which are slightly lower than the values of CO_2 capture efficiency achieved in the cases without solids recirculation but similar solid loading at the reactor inlet (i.e. cases 2 and 3 in Table 2). The presence of carbonated particles at carbonator inlet in the cases with internal solid recycle, which results in a lower amount of active CaO able to react with the CO_2, is the reason of this result. Moreover, it can be noted that specific heat for sorbent regeneration is significantly reduced by 32–47% for these cases with internal recycle compared to cases without recycle but the same solid loading at reactor inlet and comparable CO_2 capture efficiency, since the specific solid circulation between carbonator and calciner reactors is greatly reduced. As with the cases without solid internal recycle discussed before, the effect of water-wall cooled reactor has been analyzed, as shown in Fig. 6. Consistently with the previous results, the higher heat flux to the reactor walls in this case reduces the temperature along the carbonator, which makes the carbonation kinetics faster thanks to the higher driving force (i.e. lower $C_{CO_2,eq}$) and therefore increase the CO_2 capture efficiency.

In Fig. 7a and c, the distribution and conversion of the Ca-based solid population in the reactor for the cases with 50% and 66.7% recirculation ratio is shown. About 2.5 passages in the 50% recirculation case and a bit more than 3 passages for the 66.7% recirculation case are needed to convert completely the CaO to the maximum conversion of 0.2. In the 50% recirculation case, particles in the carbonator having experienced less than 3 cycles, corresponding to accumulated residence times of 9.7 and 19.4 s, remain active until the reactor exit (Fig. 7a). These particles represent the 89.4% of the total Ca-based particles. In Fig. 7b, the evolution of the single Ca particle conversion along the total reactor length is reported, showing that a total length of about 350 m (i.e. 2 passages + 70 m), corresponding to a total residence time of 24.2 s, is needed with the assumed conditions to fully convert the CaO particle to X_{max} = 20%. Similarly, for the 66.7% recirculation case (Fig. 7c), particles experiencing 1, 2 and 3 cycles, corresponding to accumulated residence times of 10.2, 20.4 and 30.6 s, remain active until the reactor exit. These active particles represent the 82.7% of the total Ca-based particles entering into the carbonator. In Fig. 7d, the evolution of the single Ca particle conversion along the total reactor length is reported, showing that a total length of about 440 m (i.e. 3 passages + 20 m) is needed with the assumed conditions to fully convert the CaO particle to X_{max} = 20%.

In Fig. 8, the effect of sorbent capacity X_{max} on the CO_2 capture efficiency curve along the reactor length is shown for the adiabatic carbonator with 50% and 66.7% of solid recirculation. The impact of sorbent capacity is significant. If sorbent capacity is reduced to 10%, CO_2 capture efficiency of only 55% would be achieved in a 140 m reactor and 66.7% of solid recycle. On the other hand, if sorbent capacity is increased to 30%, 80% capture efficiency would be more easily achieved with a reactor length between 60 and 100 m, depending on the solid loading. The increase of the CO_2 capture efficiency achieved in a 140 m long reactor with respect to the cases with X_{max} = 20% is 5–7%-points. From Fig. 8, it is evident that the benefit of high sorbent capacity tends to reduce as the reactor length increases (above roughly 60–80 m). This is due to the higher temperature reached within the reactor when CO_2 capture efficiency increases, and so the heat released from the carbonation reaction is higher, which leads to the consequent reduction of the carbonation reaction driving force (i.e. higher $C_{CO_2,eq}$).

As highlighted in Table 2 (cases 12–14), the higher sorbent capacity is also beneficial for the specific heat demand in the calciner. When sorbent capacity is increased to 30% (cases 13–14), sorbent regeneration heat reduces by about 5% compared to the corresponding cases with 20% capacity (cases 10–11) due to both the higher carbonation degree and the higher temperature reached by the carbonated solids sent back to the calciner. Both these

Table 2
Results from the simulations of the entrained flow carbonator with different operating conditions, for a total reactor length of 140 m for the gooseneck reactor and 60 m for the downflow reactor.

Case number	1	2	3	4	5	6	7	8	9	10	11	12	13	14	15	16	17	18
Type of reactor	Adiabatic, gooseneck			1 cooled reactor, gooseneck			4 cooled reactors, gooseneck			Adiabatic, gooseneck						Adiabatic, downflow		
Input variables																		
X_{max}	0.2	0.2	0.2	0.2	0.2	0.2	0.2	0.2	0.2	0.2	0.2	0.1	0.3	0.3	0.2	0.2	0.2	0.2
Inlet temperature, °C	600	600	600	600	600	600	600	600	600	600	600	600	600	600	650	600	600	600
Inlet gas velocity	15	15	15	15	15	15	15	15	15	15	15	15	15	15	15	4	4	4
Carbonator solids recirculation,%	0	0	0	0	0	0	0	0	0	50	66.7	66.7	50	66.7	66.7	0	50	66.7
Solids from calciner/gas ratio, kg/Nm^3	5	10	15	5	10	15	5	10	15	5	5	5	5	5	5	5	5	5
Specific sorbent circulation (F_{Ca}/F_{CO2})	6.6	13.2	19.8	6.6	13.2	19.8	6.6	13.2	19.8	6.6	6.6	6.6	6.6	6.6	6.6	6.6	6.6	6.6
Output variables																		
Solid/gas ratio at reactor inlet, kg/Nm^3	5	10	15	5	10	15	5	10	15	10.29	15.64	15.39	10.32	15.68	15.58	5	12.29	15.67
Reactor diameter	1.8	1.8	1.8	1.8	1.8	1.8	1.8	1.8	1.8	1.8	1.8	1.8	1.8	1.8	1.9	3.6	3.6	3.6
CO_2 capture efficiency,%	56.1	79.2	88.7	61.3	83.8	92.0	63.3	87.2	94.6	76.9	86.0	54.2	83.6	90.6	77.8	56.2	81.4	90.1
Outlet temperature, °C	723.8	699.7	678.3	673.6	666.0	651.0	608.0	621.6	616.1	693.3	671.6	646.3	700.8	675.1	714.1	753.0	709.3	680.3
Specific solid flow at reactor outlet (G_s), kg/s m^2	24.2	47.7	71.1	24.3	47.8	71.1	24.3	47.9	71.2	49.1	74.0	72.3	49.3	74.2	69.6	6.4	13.1	19.8
Sorbent conversion, $X_{carb,out}$,%	8.6	6.1	4.6	9.4	6.5	4.8	9.7	6.7	4.9	11.8	13.1	8.3	12.8	13.8	11.9	8.6	12.5	13.8
Reaction heat ($\dot{Q}_{carb}$), MW	11.0	15.5	17.4	12.0	16.5	18.0	12.4	17.1	18.5	15.1	16.9	10.3	16.4	17.8	15.3	11.0	16.0	17.7
Heat to reactor wall ($\dot{Q}_w$), MW	0	0	0	5.4	6.2	6.9	11.5	13.9	15.4	0	0	0	0	0	0	0	0	0
$\dot{Q}_w$ / $\dot{Q}_{carb}$	0	0	0	0.45	0.38	0.38	0.93	0.81	0.83	0	0	0	0	0	0	0	0	0
Heat for sorbent regeneration in the calciner (Q_{calc}), MJ/kg$_{CO2,capt}$	8.87	11.70	15.25	9.63	12.40	16.07	10.92	13.49	17.25	8.12	8.07	11.01	7.67	8.31	7.69	8.08	7.61	7.75

effects reduce the sensible heat required for solid heating in the calciner per unit of CO_2 captured.

The effect of carbonator inlet temperature can be discussed by considering case 15 in Table 2, where carbonator inlet temperature is increased from 600 to 650 °C. Compared to the corresponding case with the same sorbent capacity and recycle rate but 600 °C at the carbonator inlet (i.e. case 11), CO_2 capture efficiency reduces by 8.2% points, due to the thermodynamic limitation imposed by the higher temperature in the reactor. When solids are fed hotter in the carbonator, the temperature at which carbonation kinetics is slowed down because of the approach to chemical equilibrium is reached earlier than in the case with a lower inlet temperature. As a result, for a given reactor length, the CO_2 capture efficiency is reduced. Such result evidences the importance of keeping a sufficiently low temperature at the inlet of the adiabatic carbonator (which involves also the cooling of the recirculated solids) to enhance the driving force of the reaction along the reactor.

The possibility of having an adiabatic downflow carbonator reactor has been also assessed. Cases 16–18 in Table 2 refer to the calculations of this downflow reactor with X_{max} of 0.2 and different fractions of recirculated solids, with a total reactor length of 60 m and a gas inlet velocity of 4 m/s. Thanks to the increased solids residence time of such reactor configuration, in the cases with solids recirculation (17–18), CO_2 capture efficiency can be increased by about 4–4.5% points compared to the corresponding gooseneck reactor cases 10 and 11. Fig. 9 shows the evolution of the CO_2 capture efficiency along the reactor length for these cases. As previously observed for the cases with high sorbent capacity, the CO_2 capture efficiency evolves asymptotically to its maximum at the end of the reactor length of 60 m due to the temperature increase and therefore to the approach to equilibrium. Therefore, the achievement of higher CO_2 capture efficiencies with longer adiabatic downflow reactors results to be limited by thermodynamics.

As for the stability of the flow in the carbonator, in Fig. 10 the minimum gas velocity calculated along the single gooseneck carbonator for different cases (dots) is compared with the choking gas velocity calculated with Eqs. (20) and (21) (lines). Three groups of cases are shown, which correspond to solid to gas ratio inside the reactor of about 5, 10 and 15 kg_s/kg_g (i.e. those placed in the left, middle and right-hand sides, respectively). Black continuous line (i.e. that for a diameter of 1.85 m) corresponds to the choking velocity for the gooseneck reactor cases. Cases with solid loading around 5 kg_s/kg_g lie well above their choking line and can be therefore operated with no expected choking problem. Cases with solid loading around 10 kg_s/kg_g lie in proximity of the choking line with 20% safety margin, i.e. actual velocity is about 20% higher than the choking velocity, which has been considered a reasonable margin for ensuring dilute solid transport conditions in the reactor (Rhodes, 2008). Cases with solid loading around 15 kg_s/kg_g lie very close to the choking line, below the safety margin of 20% and a more complex high-density fluid-dynamic regime is more likely to be established in the rector under such conditions.

4. Conclusions

In this work, the 1D entrained flow carbonator model of a highly integrated Calcium looping process for cement plants has been presented and used to assess the effects of the main process parameters on the carbonator CO_2 capture efficiency and specific heat demand in the calciner. Based on the results obtained, the following main conclusions can be drawn:

- High CO_2 capture efficiencies (>80%) can be obtained in a gooseneck-type entrained-flow carbonator with a length compatible with industrial applications in cement kilns (~80

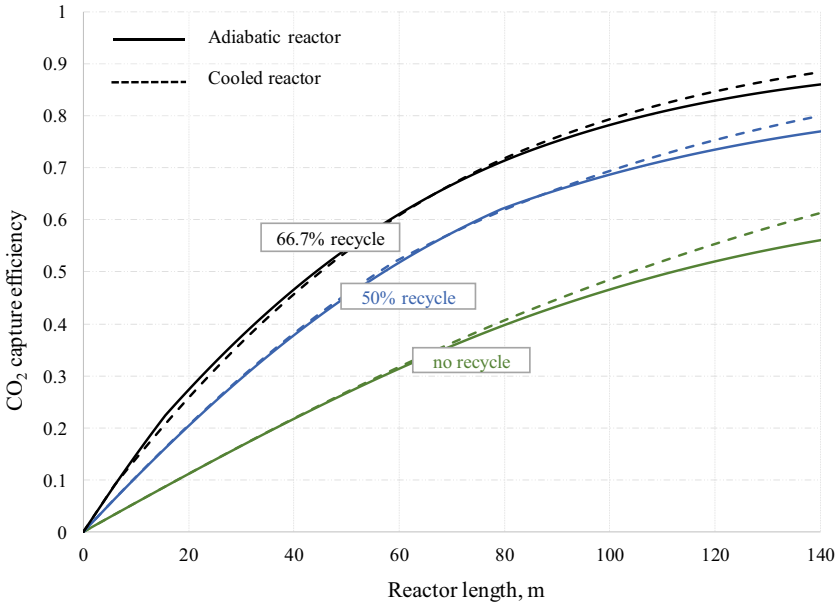

Fig. 6. CO_2 capture efficiency vs. reactor length, for adiabatic and cooled reactor, solid feeding from the calciner of 5 kg/Nm^3 and different recirculation ratios (X_{max} = 20%, inlet temperature = 600 °C).

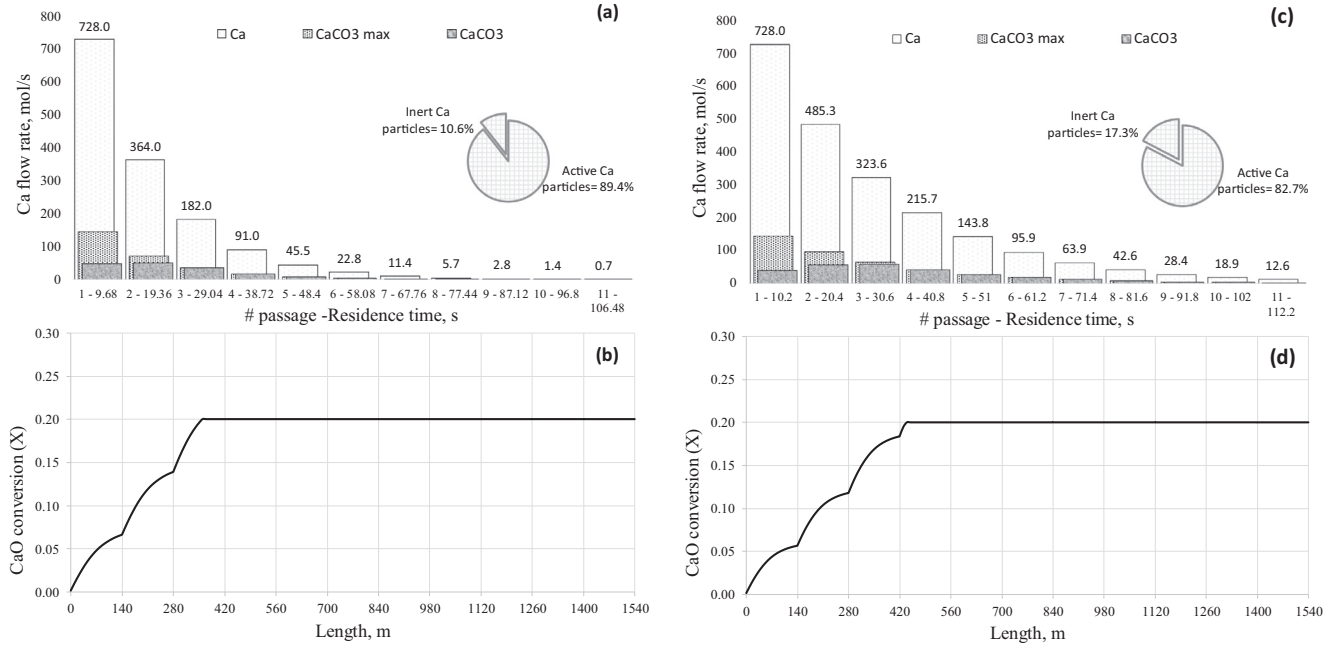

Fig. 7. Flow rate of Calcium species in solids population with different number of passages/residence time through the carbonator (a, c) and CaO to $CaCO_3$ conversion vs. total cumulative reactor length (b, d), for adiabatic reactor, solid feeding from the calciner of 5 kg/Nm^3 and 50% (a, b) and 66.7% (c, d) recirculation ratio (X_{max} = 20%, inlet temperature = 600 °C).

to 140 m). Such high CO_2 capture efficiencies can be obtained by a proper combination of sorbent capacity X_{max} and solid to gas ratio, which are the most influencing process parameters for the carbonator performance. With solid-to-gas ratio in the carbonator of ~10 kg/Nm^3 and sorbent carbonation capacity of ~20%, a length of ~120 to 140 m is required to achieve a carbonator CO_2 capture efficiency of about 80%.

- The recirculation of part of the carbonated solids at carbonator outlet back to the inlet allows increasing the solid to gas ratio in the reactor and results in similar CO_2 capture efficiency as if such solid to gas ratio were achieved by increasing the solid circulation rate from the calciner. From an energy efficiency point of view, carbonator solids recirculation is preferable with respect to the increase of calcined solids circulation because it reduces the heat demand in the calciner per kg of CO_2 captured thanks to the increased CaO carbonation degree of the carbonated solids.
- By adopting a waterwall cooled carbonator, it is possible to improve the CO_2 capture efficiency by keeping a lower reactor temperature and therefore a higher driving force for the carbonation reaction. Considering the low surface to volume ratio of a

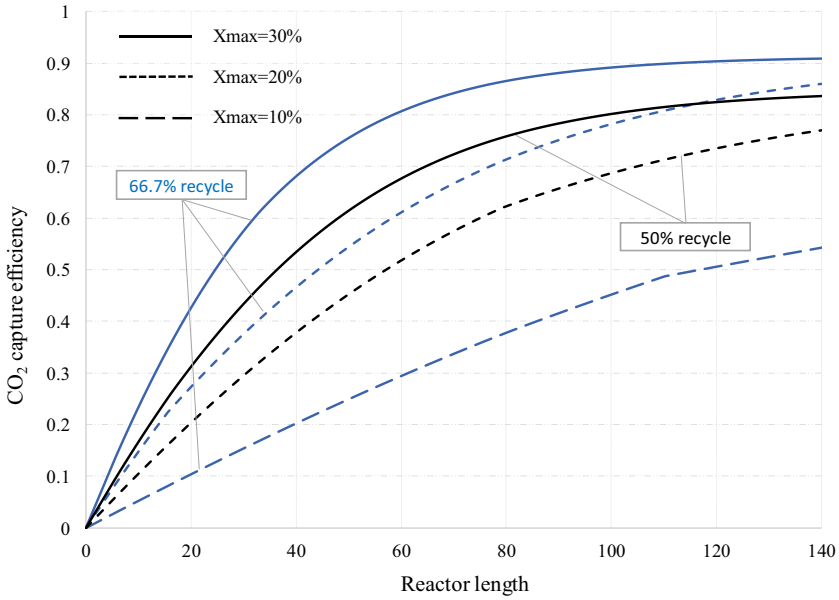

Fig. 8. CO_2 capture efficiency vs. reactor length, for adiabatic reactor, solid feeding from the calciner of 5 kg/Nm^3 and different recirculation ratios and X_{max}.

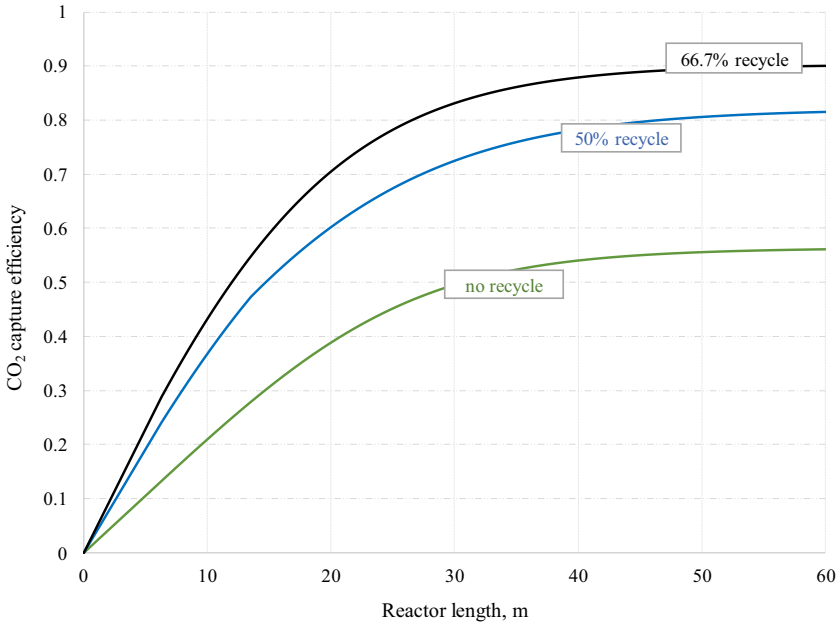

Fig. 9. CO_2 capture efficiency vs. reactor length, for downflow adiabatic reactor, solid feeding from the calciner of 5 kg/Nm^3 and different recirculation ratios.

full-scale industrial carbonator, cooling may be boosted by adopting several cooled parallel reactors (cases with up to 4 cooled parallel reactors have been assessed). The convenience of cooled vs. adiabatic carbonator should be evaluated by economic analysis. Given the modest increase of CO_2 capture efficiency (6–8% points in a 140 m long carbonator) even with 4 cooled parallel reactors compared to an adiabatic carbonator, from authors' sensibility it is likely that a simpler and cheaper adiabatic carbonator will be preferable over multiple cooled reactors.

- Temperature of the solids-gas mixture at carbonator inlet is another parameter that significantly affects the CO_2 capture efficiency of an adiabatic carbonator. It is therefore important to foresee a proper cooling of the solids both from the calciner and recirculated from the carbonator outlet to achieve an average reactants temperature of about 600 °C at the carbonator inlet.
- Downflow reactor may also be adopted as carbonator instead of a gooseneck type reactor. The downflow design allows reducing the gas velocity because solids lifting is not needed and therefore achieving higher solids residence time with lower carbonator length.
- Further experimental tests under realistic calcination conditions are needed to estimate the effect of calcination temperature and residence time and of raw meal properties on the sorbent capacity and to define calcination conditions which allow maintaining a high capacity of CaO as CO_2 sorbent. Moreover, research on the fluid-dynamics of the carbonator is also

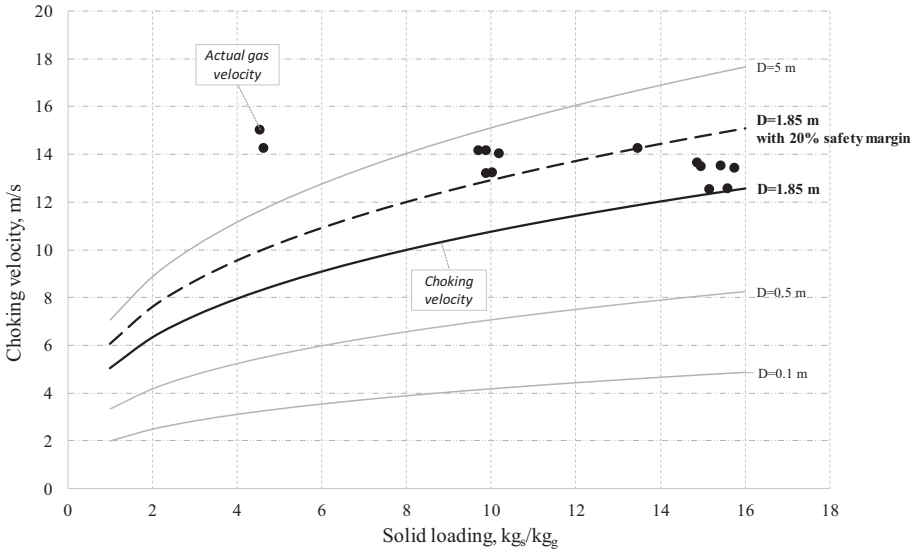

Fig. 10. Comparison between actual velocity in the assessed single gooseneck rectors and the estimated choking velocity.

needed to validate (and improve, if needed) the fluid-dynamic model, to verify the flow stability in the gooseneck carbonator and the even solids distribution in the downflow carbonator under solid/gas ratio significantly higher than in risers of conventional cement kilns.

Acknowledgements

This project has received funding from the European Union's Horizon 2020 research and innovation programme under grant agreement No. 641185 (CEMCAP).

References

Abanades, J.C., Arias, B., Lyngfelt, A., Mattisson, T., Wiley, D.E., Li, H., Ho, M.T., Mangano, E., Brandani, S., 2015. Emerging CO2 capture systems. Int. J. Greenh. Gas Control 40, 126–166. https://doi.org/10.1016/j.ijggc.2015.04.018.

Alonso, M., Álvarez Criado, Y., Fernández, J.R., Abanades, C., 2017. CO_2 carrying capacities of cement raw meals in calcium looping systems. Energy Fuels 31, 13955–13962. https://doi.org/10.1021/acs.energyfuels.7b02586.

Arias, B., Alonso, M., Abanades, C., 2017a. CO2 capture by calcium looping at relevant conditions for cement plants: experimental testing in a 30 kW_{th} pilot plant. Ind. Eng. Chem. Res. 56, 2634–2640. https://doi.org/10.1021/acs.iecr.6b04617.

Arias, B., Diego, M.E., Abanades, J.C., Lorenzo, M., Diaz, L., Martínez, D., Alvarez, J., Sánchez-Biezma, A., 2013. Demonstration of steady state CO2 capture in a 1.7 MW_{th} calcium looping pilot. Int. J. Greenh. Gas Control 18, 237–245. https://doi.org/10.1016/j.ijggc.2013.07.014.

Arias, B., Turrado, S., Alonso, M., Marbán, G., Abanades, C., 2017b. Results of entrained flow carbonator/calciner tests. CEMCAP project Deliverable D12.2. https://www.sintef.no/projectweb/cemcap/results/.

Atsonios, K., Grammelis, P., Antiohos, S.K., Nikolopoulos, N., Kakaras, E., 2015. Integration of calcium looping technology in existing cement plant for CO2 capture: process modeling and technical considerations. Fuel 153, 210–223. https://doi.org/10.1016/j.fuel.2015.02.084.

Barker, R., 1973. Reversibility of the reaction CaCO3 ↔ CaO + CO2. J Appl. Chem. Biotechnol. 23, 733–742.

Campanari, S., Cinti, G., Consonni, S., Fleiger, K., Gatti, M., Hoppe, H., Martínez, I., Romano, M., Spinelli, M., Voldsund, M., 2016. Design and performance of CEMCAP cement plant without CO2 capture. CEMCAP project Deliverable D4.1. www.sintef.no/projectweb/cemcap/results/.

CEMCAP, 2016. CEMCAP EU H2020 Project. www.sintef.no/cemcap/.

Chambers, A.J., Marcus, R.D., 1986. Pneumatic Conveying Calculations. In: Second International Conference on Bulk Materials Storage, Handling and Transportation. pp. 49–52.

Danziger, W.J., 1963. Heat transfer to fluidized gas-solids mixtures in vertical transport. Ind. Eng. Chem. Process Des. Dev. 2, 269–276. https://doi.org/10.1021/i260008a003.

De Lena, E., Spinelli, M., Martínez, I., Gatti, M., Scaccabarozzi, R., Cinti, G., Romano, M.C., 2017. Process integration study of tail-end Ca-looping process for CO_2 capture in cement plants. Int. J. Greenh. Gas Control 67, 71–92. https://doi.org/10.1016/j.ijggc.2017.10.005.

Dean, C.C., Blamey, J., Florin, N.H., Al-Jeboori, M.J., Fennell, P.S., 2011. The calcium looping cycle for CO_2 capture from power generation, cement manufacture and hydrogen production. Chem. Eng. Res. Des. 89, 836–855. https://doi.org/10.1016/j.cherd.2010.10.013.

Drew, T.B., Koo, E.C., McAdams, W.H., 1932. The friction factors for clean round pipes. Trans. AIChE J. 28, 56–72.

Gardiner, W.C., 1984. Combustion Chemistry. Springer-Verlag, New York.

Geldart, D., 1973. Types of gas fluidization. Powder Technol. 7. https://doi.org/10.1016/0032-5910(73)80037-3.

Grasa, G., Murillo, R., Alonso, M., Abanades, J.C., 2009. Application of the random pore model to the carbonation cyclic reaction. AIChE J. 55, 1246–1255. https://doi.org/10.1002/aic.11746.

Grasa, G.S., Abanades, J.C., 2006. CO2 capture capacity of CaO in long series of carbonation/calcination cycles. Ind. Eng. Chem. Res. 45, 8846–8851. https://doi.org/10.1021/ie0606946.

Hoenig, V., Hoppe, H., Koring, K., Lemke, J., 2012. ECRA CCS Project – Report on Phase III. TR-ECRA-119/2012.

Hornberger, M., Spörl, R., Scheffknecht, G., 2017. Calcium Looping for CO2 Capture in Cement Plants – Pilot Scale Test. Energy Procedia 114, 6171–6174. http://doi.org/10.1016/j.egypro.2017.03.1754.

NASA ThermoBuild, 2017. http://www.grc.nasa.gov/WWW/CEAWeb/ceaThermoBuild.htm. Accessed in 2017.

Incropera, F.P., DeWitt, D.P., Bergman, T.L., Lavine, A.S., 2007. Fundamentals of Heat and Mass Transfer, Water, Dekker Mechanical Engineering. John Wiley & Sons.

Konno, H., Saito, S., 1969. Pneumatic conveying of solids though straight pipes. J. Chem. Eng. Jpn. 2, 211–217.

Kremer, J., Galloy, A., Ströhle, J., Epple, B., 2013. Continuous CO2 capture in a 1-MWth carbonate looping pilot plant. Chem. Eng. Technol. 36, 1518–1524. https://doi.org/10.1002/ceat.201300084.

Marchi, M.I., Cinti, G., Romano, M.C., Campanari, S., Consonni, S., 2012a. Improved process for the production of cement clinker and related apparatus (in Italian). Patent MI2012 A00382.

Marchi, M.I., Cinti, G., Romano, M.C., Campanari, S., Consonni, S., 2012b. Process and improved plant for the production of cement clinker (in Italian). Patent MI2012 A00383.

Martínez, I., Grasa, G., Parkkinen, J., Tynjälä, T., Hyppänen, T., Murillo, R., Romano, M. C., 2016. Review and research needs of Ca-Looping systems modelling for post-combustion CO2 capture applications. Int. J. Greenh. Gas Control 50, 271–304. https://doi.org/10.1016/j.ijggc.2016.04.002.

Olivier, J.G.J., Janssens-Maenhout, G., Muntean, M., Peters, J.A.H.W., 2016. Trends in global CO2 emissions: 2016 report, The Hague: PBL Netherlands Environmental Assessment Agency; Ispra: European Commission, Joint Research Centre.

Ozcan, D.C., Ahn, H., Brandani, S., 2013. Process integration of a Ca-looping carbon capture process in a cement plant. Int. J. Greenh. Gas Control 19, 530–540. https://doi.org/10.1016/j.ijggc.2013.10.009.

Pathi, S.K., Lin, W., Illerup, J.B., Dam-Johansen, K., Hjuler, K., 2013. CO2 capture by cement raw meal. Energy Fuels 27. https://doi.org/10.1021/ef401073p.

Pfeffer, R., Rossetti, S., Lieblein, S., 1966. Analysis and correlation of heat-transfer coefficient and friction factor data for dilute gas-solid suspensions. NASA technical note.

Rajan, K.S., Dhasandhan, K., Srivastava, S.N., Pitchumani, B., 2008. Studies on gas–solid heat transfer during pneumatic conveying. Int. J. Heat Mass Transf. 51, 2801–2813. https://doi.org/10.1016/j.ijheatmasstransfer.2007.09.042.

Rajan, K.S., Srivastava, S.N., Pitchumani, B., Mohanty, B., 2006. Simulation of gas–solid heat transfer during pneumatic conveying: Use of multiple gas inlets along the duct. Int. Commun. Heat Mass Transf. 33, 1234–1242. https://doi.org/10.1016/j.icheatmasstransfer.2006.06.011.

Rhodes, M., 2008. Introduction to Particle Technology: Second Edition, Introduction to Particle Technology: 2nd ed. http://doi.org/10.1002/9780470727102.

Rodríguez, N., Murillo, R., Abanades, J.C., 2012. CO2 capture from cement plants using oxyfired precalcination and/or calcium looping. Environ. Sci. Technol. 46, 2460–2466. https://doi.org/10.1021/es2030593.

Romano, M.C., Spinelli, M., Campanari, S., Consonni, S., Marchi, M., Pimpinelli, N., Cinti, G., 2014. The calcium looping process for low CO_2 emission cement plants. Energy Procedia 61, 500–503. https://doi.org/10.1016/j.egypro.2014.11.1158.

Shimizu, T., Hirama, T., Hosoda, H., Kitano, K., Inagaki, M., Tejima, K., 1999. A twin fluid-bed reactor for removal of CO2 from combustion processes. Chem. Eng. Res. Des. 77, 62–68. https://doi.org/10.1205/026387699525882.

Spinelli, M., Martínez, I., De Lena, E., Cinti, G., Hornberger, M., Spörl, R., Abanades, J. C., Becker, S., Mathai, R., Fleiger, K., Hoenig, V., Gatti, M., Scaccabarozzi, R., Campanari, S., Consonni, S., Romano, M.C., 2017. Integration of ca-looping systems for CO_2 capture in cement plants. Energy Procedia 114, 6206–6214. https://doi.org/10.1016/j.egypro.2017.03.1758.

Stull, D.R., Prophet, H., 1971. JANAF Thermochemical Tables. National Bureau of Standards, Washington D.C., USA.

The Mathworks Inc., n.d. Matlab, v. R2017a.

ZEP, 2013. CO2 Capture and Storage (CCS) in Energy-intensive Industries – An Indispensable Route to an EU Low-carbon Economy, 38.